Journal of Electronic Materials (2023) 52:679–690
https://doi.org/10.1007/s11664-022-10038-6

ORIGINAL RESEARCH ARTICLE

Origin of Double-Rhombic Single Shockley Stacking Faults in 4H-SiC Epitaxial Layers

Johji Nishio[1] · **Chiharu Ota**[1] · **Ryosuke Iijima**[1]

Received: 19 July 2022 / Accepted: 11 October 2022 / Published online: 31 October 2022
© The Minerals, Metals & Materials Society 2022

Abstract

We have investigated double-rhombic single Shockley stacking faults (DRSFs) in 4H-SiC epitaxial layers by analyzing structural details. A combination of plan-view transmission electron microscopy (TEM) and cross-sectional high-angle annular dark field scanning TEM made it possible to determine the Burgers vectors of partial dislocations that consist of DRSF boundaries and the type of glide of the original basal plane dislocations (BPDs). From these results, the origins of DRSFs were identified as BPDs that originated as 60-degree perfect dislocations, and the inclination of the DRSFs was found to depend on the Burgers vectors and the type of glide of the original BPDs. Also, the configuration of the accompanying threading edge dislocations (TEDs) at both ends of the BPDs was categorized into two types, namely (1) TEDs at both ends of the BPD segments toward the surface of the epitaxial layer (cis-configuration) which form the half-loop arrays, and (2) a TED at one end of the BPD from the deeper side of the epitaxial layer and another toward the surface of the epitaxial layer (trans-configuration), and the original BPD segments were isolated. The shrinking processes of the DRSFs were also examined, and it was found that they were not a reversal of the expansion process.

Keywords 4H-SiC · forward degradation · single Shockley stacking fault · partial dislocation · transmission electron microscopy

Introduction

Problems such as forward voltage degradation and reduced blocking voltage that are observed mainly in bipolar devices and even in metal–oxide–semiconductor field-effect transistors (MOSFETs) fabricated on 4H silicon carbide (SiC) with a *p*–*n* junction in the structure are widely known to be attributable to the expansion of single Shockley-type stacking faults (1SSFs) in the epitaxial layer that originate from basal plane dislocations (BPDs).[1] Although many studies have proposed concepts for preventing the expansion of 1SSFs, such as reducing the minority carrier lifetime in the recombination-enhancing layers,[2] BPDs are still present in commercially available epitaxial layers and cause variation in the threshold current density for 1SSF expansion. We consider that the structural difference in 1SSFs might be the key for better understanding the relation with electrical properties.[3–5] The expanding shapes can be explained by the different combinations of partial dislocations (PDs) surrounding 1SSFs.[6–9]

It was reported that half-loop arrays (HLAs) of the dislocations consist of short BPD segments and they are accompanied by two threading edge dislocations (TEDs) penetrating to the epilayer surface on both ends.[10–17] Double-rhombic shapes on 1SSFs originating from HLAs have been observed by photoluminescence (PL) imaging after ultraviolet (UV) illumination and electron-beam-induced current images.[18–21] In a recent work, we investigated the structure of double-rhombic 1SSFs (DRSFs) to identify the Burgers vectors, core species, and type of glide of the constituent PDs, and found that these are another type of BPD segment that has TEDs on both ends, one of which is from the deeper side of the epilayer.[21]

In this paper, we discuss these two characteristic structures of the BPD segments, which have not been investigated experimentally yet, as the origins of DRSFs with different inclinations. The shrinking processes of both DRSFs are

✉ Johji Nishio
johji.nishio@toshiba.co.jp

[1] Corporate Research and Development Center, Toshiba Corporation, 1 Komukai Toshiba-Cho, Saiwai-Ku, Kawasaki 212-8582, Japan

also examined and it is found that they are not a reversal of the expansion process.

Experimental Procedures

The epitaxial layers examined in this study were approximately 30 μm-thick and grown on 4H-SiC *n*-type 4°off-cut (0001) substrate. PL imaging was carried out using a Hg-Xe lamp filtered with a 313 nm band-pass filter as an excitation source. An area of 0.36 cm^2 was illuminated at an excitation power density of about 1.53 Wcm^{-2}.[5,22,23] Two types of double-rhombic 1SSFs (which we labeled DRSF-A and DRSF-B) that have different inclination angles were selected by PL imaging and expanded by UV illumination for 30 min. Structural analysis was carried out by plan-view and cross-sectional transmission electron microscopy (TEM). To examine the fine structure of BPDs and 1SSFs, TEM sample preparation must first be performed by a focused ion beam (FIB) technique. For this, the depth of the 1SSF in the epilayer needs to be determined precisely. Estimation from PL imaging can be misleading in terms of depth because the shallowest end of a BPD is not always located at the very surface of the epilayer. Therefore, in this work, preliminary cross-sectional TEM specimens were sampled in locations that contained identical 1SSFs sufficiently far from the areas where structural analysis is desired. Based on the 1SSFs depth results, plan-view TEM samples were prepared by FIB. The Burgers vectors for PDs surrounding DRSFs were determined based on the plan-view TEM images by the extinction rule under two-beam conditions using three different diffraction vectors, $\boldsymbol{g}$, of $11\bar{2}0$, $1\bar{2}10$, and $\bar{2}110$ on the FIB-sampled specimens at an acceleration voltage of 300 kV. From the plan-view TEM images, different sampling points were determined for the following analyses of cross-sectional scanning TEM (STEM) for high-resolution high-angle annular dark-field scanning TEM (HAADF-STEM). The HAADF-STEM images help determine the core species and the Burgers vectors ($\boldsymbol{b}$) of PDs using the results obtained beforehand by the $\boldsymbol{g}\cdot\boldsymbol{b}$ contrast analysis of the plan-view TEM observation.

Results and Discussion

Figure 1a and b show PL images of the DRSFs using a bandpass filter (BPF) of 420 nm (FWHM: 10 nm) to detect 1SSFs.[24] Plan-view TEM sampling positions are shown by broken lines in Fig. 1, and the corresponding schematic shapes of the DRSFs are illustrated below the PL images. The DRSF-A in Fig. 1a is thought to have expanded from the BPDs lined up as an HLA, each of which is accompanied by a pair of DRSFs with similar shapes, whereas the inclined DRSF-B in Fig. 1b was isolated.

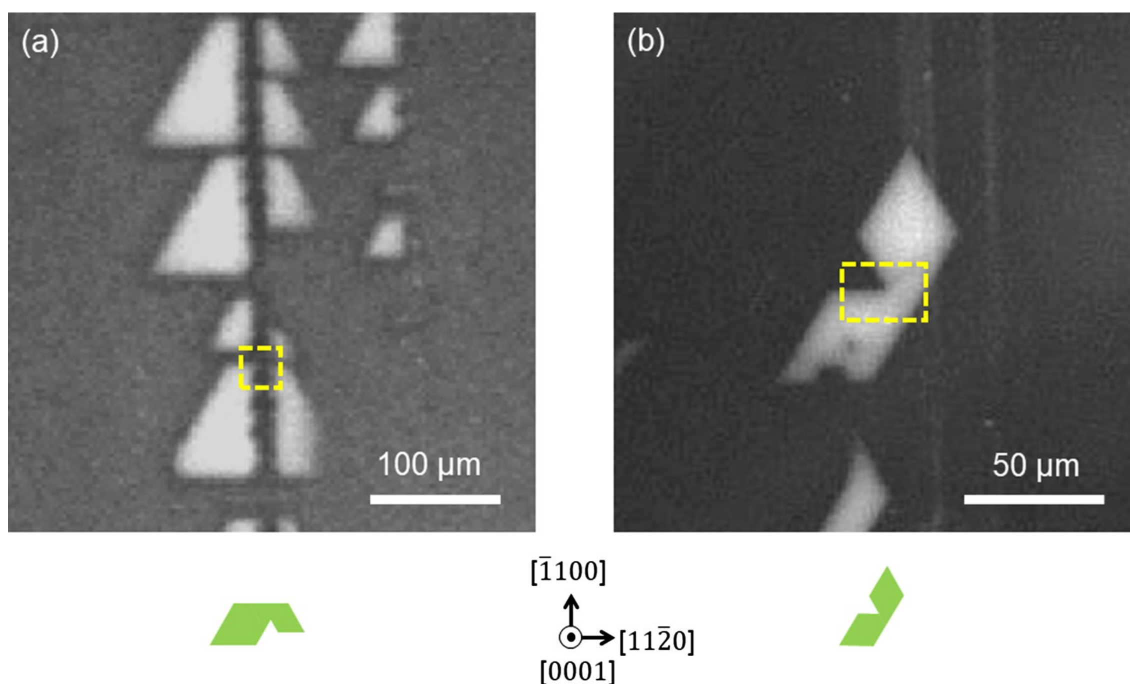

Fig. 1 PL images taken with a 420-nm BPF, schematics of DRSFs, and sampling positions for plan-view TEM observations: (a) DRSF-A and (b) DRSF-B.

Figure 2a shows the bright-field (BF) plan-view TEM images of DRSF-A at relatively low magnification acquired with the aim of maximizing the 1SSF contrast, with a slight inclination of the sample toward the $\left[11\overline{2}0\right]$ direction from the [0001] zone axis. Figure 2b shows an enlarged plan-view BF-TEM image of the upper-right part of the DRSF-A in Fig. 2a. In Fig. 2, the darker area corresponds to a 1SSF. Although DRSF-A contracted and changed shape from that observed in the PL image shown in Fig. 1a, this phenomenon was also observed in low-power UV illumination for HLA-oriented DRSFs[25] and triangular 1SSFs.[26] Figure 3a, b, and c show the enlarged plan-view BF-TEM images of the upper-right part of the DRSF-A in Fig. 2. Figure 3 shows the results of $\boldsymbol{g}\cdot\boldsymbol{b}$ contrast analysis under two-beam conditions. Selected area electron diffraction patterns are also inserted on the corresponding plan-view TEM images. In Fig. 3b, the dislocation line contrast disappeared on the left half, whereas in Fig. 3c, the dislocation line contrast disappeared on the

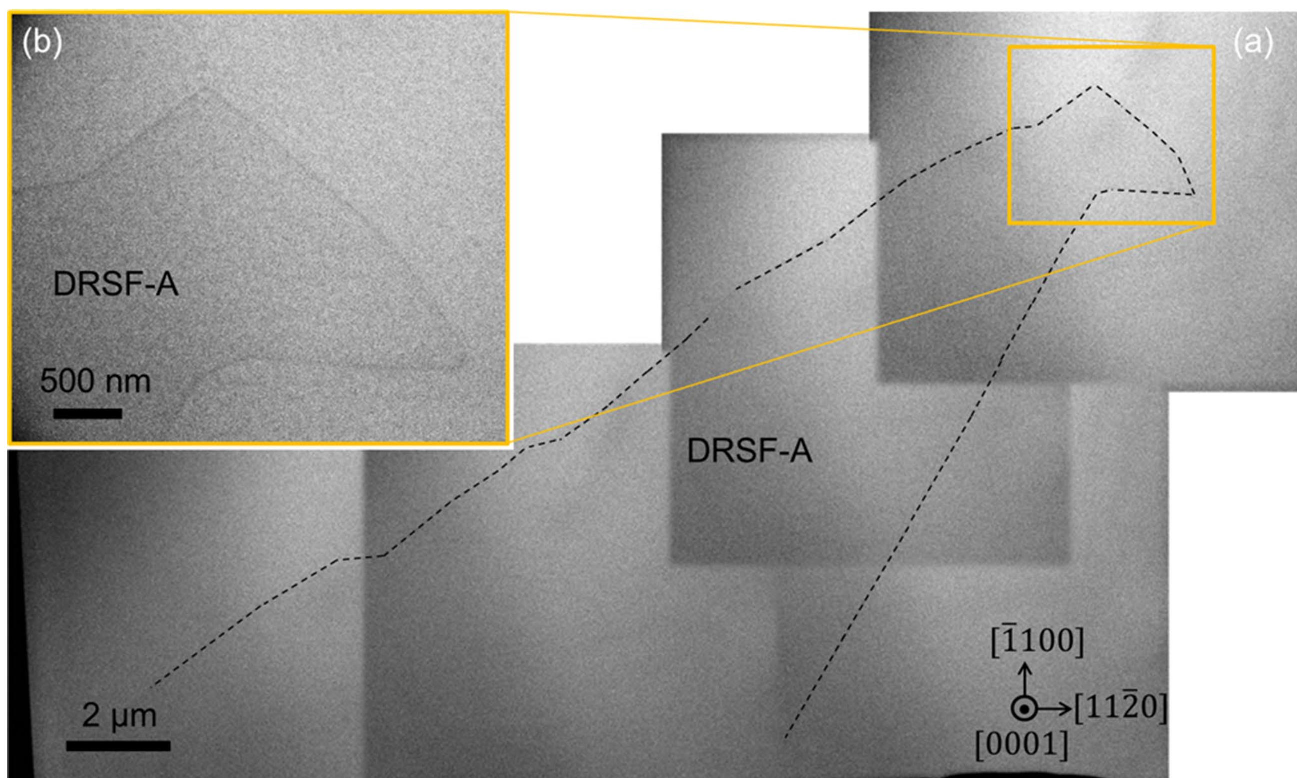

Fig. 2 BF plan-view TEM images for DRSF-A: (a) low magnification and (b) enlarged part.

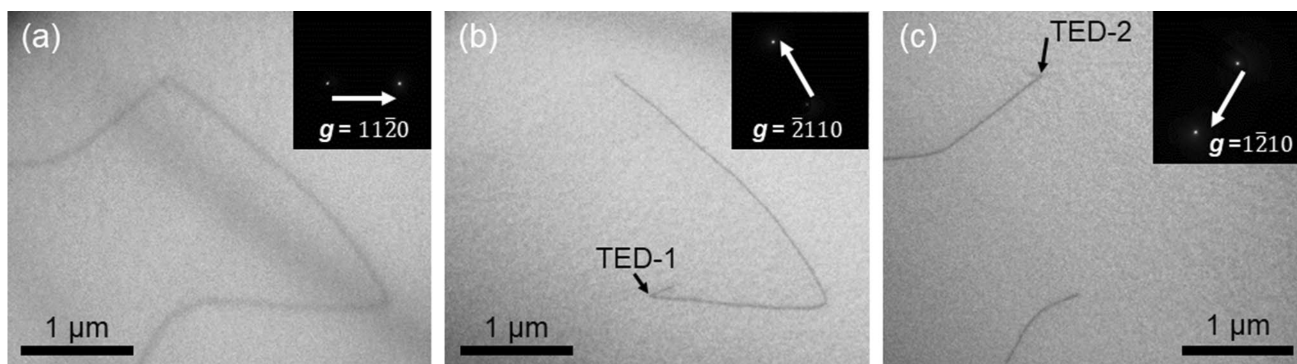

Fig. 3 BF plan-view TEM results of $\boldsymbol{g}\cdot\boldsymbol{b}$ contrast analysis for DRSF-A: (a) $\boldsymbol{g}=11\overline{2}0$, (b) $\boldsymbol{g}=\overline{2}110$, and (c) $\boldsymbol{g}=1\overline{2}10$.

right half. This indicates that the left and right dislocation loops have $\boldsymbol{b}$ of $\pm\left[01\overline{1}0\right]$ and $\pm\left[10\overline{1}0\right]$, respectively. Furthermore, in Fig. 3b and c, short beard-like lines are observed as indicated by arrows. These features are typical of TEDs, as also observed in the triangular 1SSF expanded from the deeper BPD part of the BPD-TED converted origin.[5] Therefore, the connecting points of the dislocation loops are considered to have TEDs, and these TEDs are located at the edge positions of the initial unexpanded BPD segment. The structural results for DRSF-A are summarized in Fig. 4. It can be seen that the Burgers vectors changed from $\pm(1/3)\left[01\overline{1}0\right]$ on the left PD loop to $\pm(1/3)\left[10\overline{1}0\right]$ on the right PD loop at TED-1 and TED-2. For simplicity, the dark green dashed line in Fig. 4 represents the estimated initial BPD as a straight line. The resultant $\boldsymbol{b}$ of the PDs determined by the $\boldsymbol{g}\cdot\boldsymbol{b}$ contrast analysis are shown by bidirectional arrows and the composite Burgers vector of the original BPD is also given. In Fig. 4, the following cross-sectional HAADF-STEM sampling position (#1) and the observation direction are also depicted by blue broken lines and a blue arrow, respectively.

Figure 5a shows the BF plan-view TEM images of DRSF-B at relatively low magnification acquired with the aim of maximizing the 1SSF contrast, with a slight inclination of the sample toward the $\left[11\overline{2}0\right]$ direction from the [0001] zone axis. Figure 5b and c show enlarged plan-view BF-TEM images of the right and left rectangular parts of DRSF-B in Fig. 5a, respectively. In Fig. 5, the darker area corresponds to a 1SSF. DRSF-B contracted and changed shape from that observed in the PL image shown in Fig. 1b, as in DRSF-A. Figure 6 shows the results of $\boldsymbol{g}\cdot\boldsymbol{b}$ contrast analysis under two-beam conditions. In Fig. 6, selected area electron diffraction patterns are also inserted on the corresponding plan-view TEM images. In Fig. 6a and d, the dislocation line contrast disappeared on the upper half, whereas in Fig. 6b and e, the dislocation line contrast disappeared on the left half. These indicate that the upper and left dislocation loops have $\boldsymbol{b}$ of $\pm\left[1\overline{1}00\right]$ and $\pm\left[0\overline{1}10\right]$, respectively. Furthermore, in Fig. 6b and d, short beard-like lines are observed and are indicated by arrows. These features are typical of TEDs, as also observed in DRSF-A in Fig. 3. In Fig. 7, it can be seen that the Burgers vectors changed from $\pm(1/3)\left[0\overline{1}10\right]$ on the left PD loop to $\pm(1/3)\left[1\overline{1}00\right]$ on the upper PD loop at TED-3 and TED-4. Therefore, the connecting points of the dislocation loops are thought to have TEDs, and these TEDs are

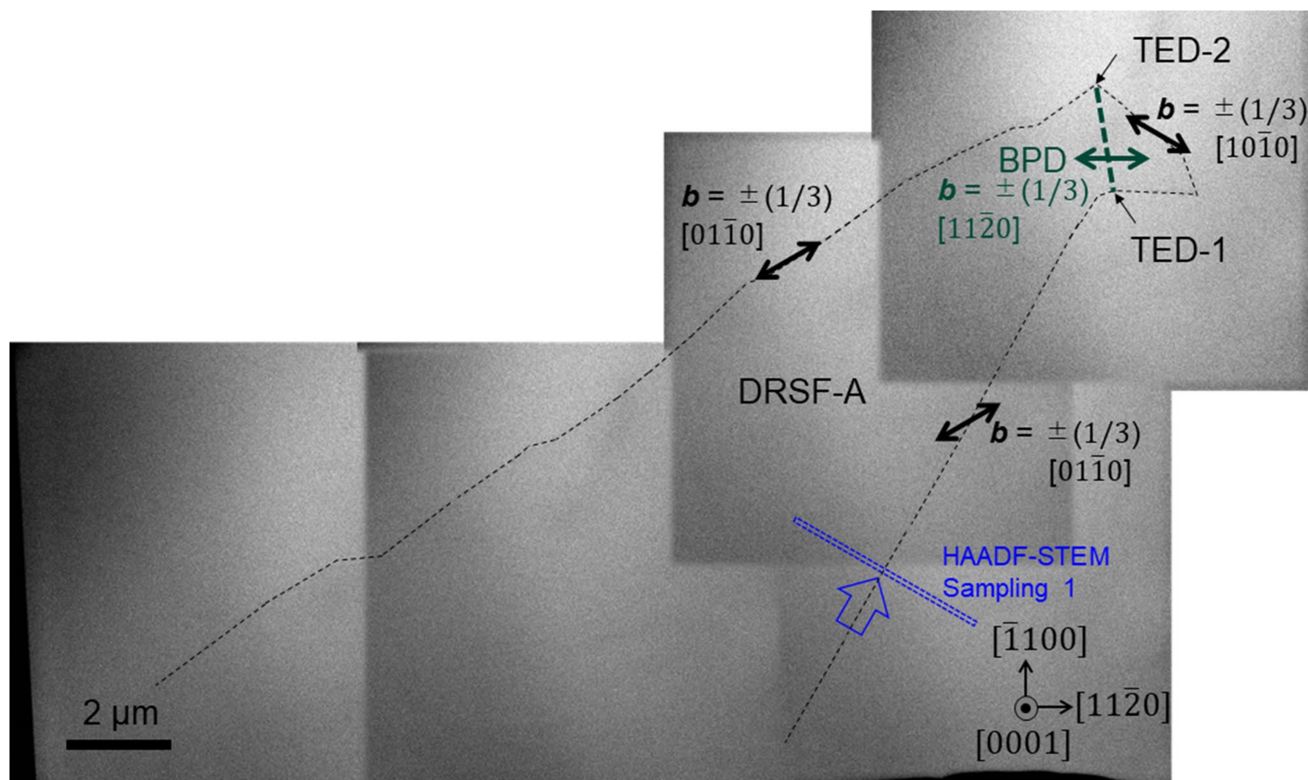

Fig. 4 Composite image of BF plan-view TEM images with low magnification showing Burgers vectors of PDs and initial BPD obtained from $\boldsymbol{g}\cdot\boldsymbol{b}$ contrast analysis for DRSF-A, estimated initial BPD position, and the following HAADF-STEM sampling position and the observation direction.

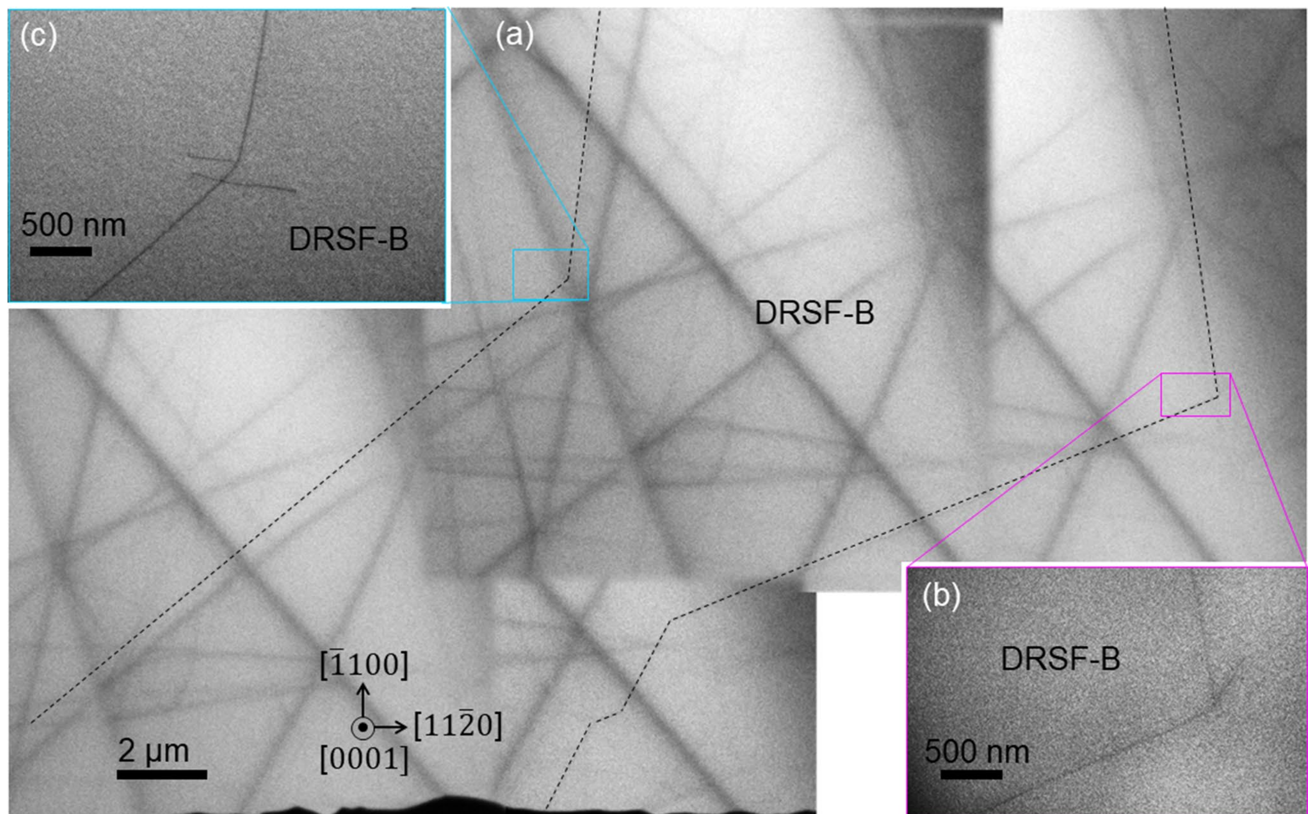

Fig. 5 BF plan-view TEM images of DRSF-B: (a) low magnification, (b) enlarged part of the right corner, and (c) enlarged part of the left corner.

located at the edge positions of the initial unexpanded BPD segment. The structural data for DRSF-B are summarized in Fig. 7. For simplicity, the dark green dashed line in Fig. 7 represents the estimated initial BPD as a straight line. The resultant ***b*** of the PDs determined by the ***g·b*** contrast analysis are shown by bidirectional arrows and the composite Burgers vector of the original BPD is also given. In Fig. 7, the following cross-sectional HAADF-STEM sampling positions (#2 and #3) and the observation directions are also depicted by blue broken lines and blue arrows, respectively.

Figure 8a, b, and c show cross-sectional HAADF-STEM images and the resulting Burgers circuits of each core of the PD at "HAADF-STEM Sampling #1" in Fig. 4, and "HAADF-STEM Sampling #2," and "HAADF-STEM Sampling #3" in Fig. 7, where the position was determined by the edge of each 1SSF as determined by BF-TEM observation.

As shown in Fig. 8a, the number of atoms on the upper side of the Burgers circuit is one less than that on the lower side. This indicates that the extra-half plane is on the C-face side; in other words, the PD has a C-core. According to the finish-to-start using the right-hand definition in the perfect crystal convention, the Burgers vectors were determined to be the directions from B to A in the Burgers circuit shown in Fig. 8a. When the circuit is viewed from (0001), alternative directions are possible between $\left[01\bar{1}0\right]$ or $\left[1\bar{1}00\right]$. Considering the result of the possible Burgers vector of $\left[01\bar{1}0\right]$ or $\left[0\bar{1}10\right]$ obtained by ***g·b*** contrast analysis of the plan-view TEM, the Burgers vector that satisfies both of these is uniquely obtained as (1/3) $\left[01\bar{1}0\right]$. Likewise, Fig. 8b and c show that the core structures are Si- and C-cores and the Burgers vectors are (1/3) $\left[\bar{1}100\right]$ and

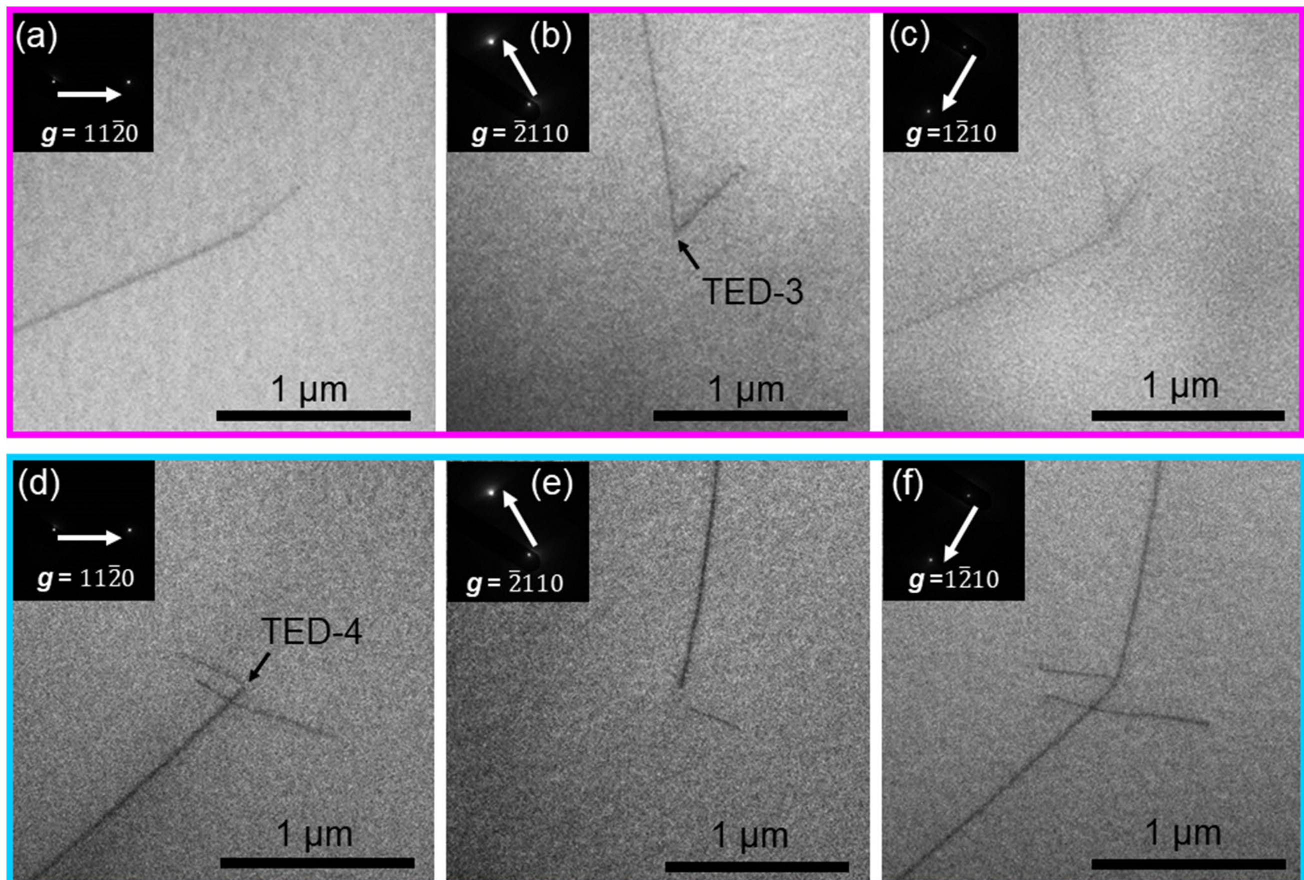

Fig. 6 BF plan-view TEM results of $\boldsymbol{g}\cdot\boldsymbol{b}$ contrast analysis for DRSF-B at the right connecting point of the PDs (upper column) and at the left connecting point of the PDs (lower column): (a) and (d) $\boldsymbol{g}=11\bar{2}0$, (b) and (e) $\boldsymbol{g}=\bar{2}110$, and (c) and (f) $\boldsymbol{g}=1\bar{2}10$.

(1/3) $\left[01\bar{1}0\right]$ for the respective PDs. In the case of DRSF-A, the original BPDs of HLAs were reported to be perfect dislocations with a Burgers vector of (1/3) $\left[11\bar{2}0\right]$.[10,11] Once the Burgers vector of a Shockley pair of PDs is found to be $\left[01\bar{1}0\right]$ as in Fig. 8a, the other pair is necessarily $\left[10\bar{1}0\right]$. This is self-evident and does not require experimental examination. However, the inclined DRSF needs to be analyzed due to the lack of information about the composite ***b*** for the original BPDs. In the DRSF-B case, according to the results for the ***b*** for the PDs obtained as shown in Fig. 7, ***b*** of the original unexpanded BPD is expected to be a composite of two ***b*** of the PDs, namely, (1/3) $\left[1\bar{2}10\right]$. At each HAADF-STEM sampling point shown in Figs. 4 and 7, the layers where each 1SSF is located were found to have tetrahedrons facing toward $\left[\bar{1}010\right]$, $\left[01\bar{1}0\right]$, and $\left[\bar{1}010\right]$ on the non-faulted side as depicted by the bold outlines in Fig. 8a, b, and c, respectively. When we look at the tetrahedrons on the $\left(11\bar{2}0\right)$ face, they are all facing $[1\bar{1}00]$. This viewpoint is essential for determining the glide-type information.[27,28] The type of glide was categorized by the layer that contains the rotational glide: type A for the BPD loop on either layer with tetrahedrons facing the $\left[\bar{1}100\right]$ direction, and type B for the BPD loop on either layer with tetrahedrons facing the $\left[1\bar{1}00\right]$ direction, when looking at $\left(11\bar{2}0\right)$. The types of glide were found to be type B for BPDs that expanded to both DRSF-A and DRSF-B. As far as we know, this is the first direct experimental procedure to determine the type of glide using high-resolution HAADF-STEM images acquired on any $\left(11\bar{2}0\right)$ planes.

The uniquely obtained ***b*** of the PDs makes it possible to determine the detailed structure of DRSF-A and DRSF-B, as illustrated in Fig. 9. In Fig. 9, three-dimensional schematic

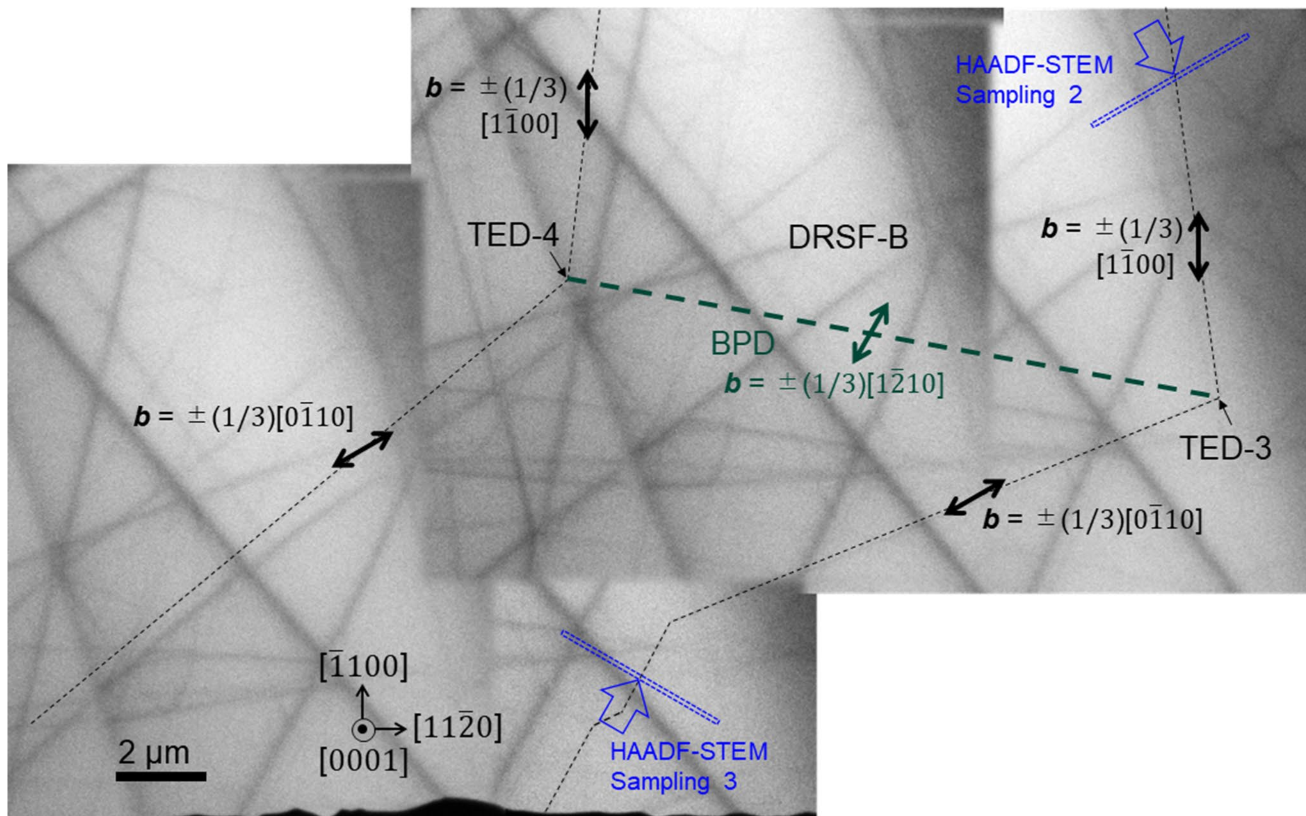

Fig. 7 Composite image of BF plan-view TEM images with low magnification showing Burgers vectors of PDs and initial BPD obtained from ***g·b*** contrast analysis for DRSF-B, estimated initial BPD position, and the following HAADF-STEM sampling positions and the observation directions.

structures of the original unexpanded BPDs, DRSFs observed by PL imaging after expansion by UV illumination, and shrunken shape by FIB sampling or TEM observation are shown. It should be noted that only the shrunken PD shapes cannot give clues about whether they are Si-core or C-core PDs, because our basic understanding of the mobility of Si-core and C-core PDs at room temperature is no longer useful. Apparently, from the shrunken 1SSF shapes as observed in Figs. 2 and 5, the shrinking process was not found to obey the way it expanded. This tendency was also reported for bar-shaped 1SSFs.[29,30] This implies that the expansion criteria are no longer useful for distinguishing mobile Si-core and immobile C-core PDs in the shrinking process. When observing the shrinking 1SSF shape, great care is needed to judge the core species just by the way they contract. Previous reports on the possibility of C-core PD movement at room temperature might also hinder our understanding of the phenomena.[31–33]

The experimentally determined ***b*** of each PD and estimated original BPD positions are shown as light-blue arrows and dashed dark green lines, respectively, in the plan-view BF-TEM images in Fig. 10a and b, and their running directions are also shown in the corresponding dislocation loop models.[27,28] As seen in Fig. 9, the original BPDs have two TEDs but with different directions at both ends. The configuration of the accompanying TEDs at both ends of the BPDs can be categorized into two types: (1) TEDs at both ends of the BPD segments are toward the surface of the epitaxial layer (cis-configuration) that appeared on DRSF-A and (2) a TED at one end of the BPD is from the deeper side of the epitaxial layer and another is toward the surface of the epitaxial layer (trans-configuration) appeared on DRSF-B. Both structures were previously confirmed experimentally by cross-sectional TEM analysis.[21] Considering that inclined DRSF like DRSF-B was isolated as shown in Fig. 1, the formation mechanism might be different from the BPDs with cis-configuration of TEDs on the HLAs. The mechanism by which the trans-configuration of TEDs could form has been discussed based on the results of unstable step flow during the epitaxial growth process.[21]

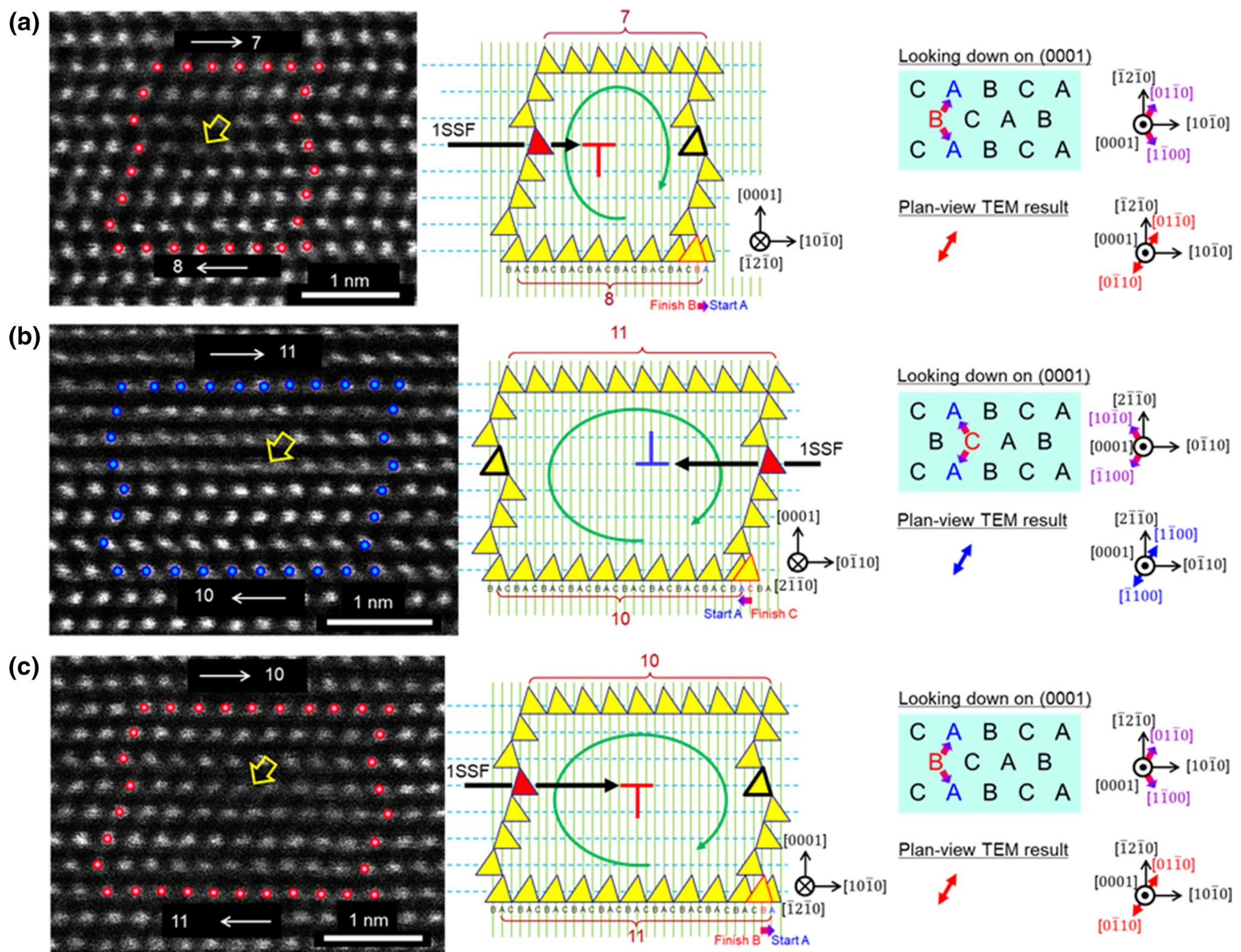

Fig. 8 Cross-sectional HAADF-STEM images and their interpretations for uniquely determining Burgers vectors at each PD: (a) HAADF-STEM Sampling 1 on DRSF-A in Fig. 4, (b) HAADF-STEM Sampling 2, and (c) HAADF-STEM Sampling 3 on DRSF-B in Fig. 7.

The inclination of the estimated original BPD lines suggests that each BPD consisted of dominant and sub-dominant lines of BPDs as shown by the yellow arrows in Fig. 10, based on the idea that the segments of the PD loop lie in the Peierls valleys along the $< 11\bar{2}0 >$ directions.[34,35] In the cases of both DRSF-A and DRSF-B, the original BPDs were found to be perfect 60-degree dislocations as noticed from the dislocation loop model, even consisting of possible combinations of two running directions, ξ. The trans-configuration of TEDs was also found and confirmed the structure by cross-sectional TEM study on a triangular 1SSF having an origin near the surface of the epitaxial surface.[8] Despite having the same trans-configuration TEDs, the expanded 1SSF shape difference can be explained by the combination of PDs at the originated BPDs; a triangular 1SSF from a perfect screw BPD in which the PDs consist of 30° Si-core and 30°C-core, and a DRSF from a perfect 60-degree BPD of which PDs consist of 30° Si-core and 90° Si-core.

The schematics of all possible DRSF shapes are summarized in Table I, with the structural parameters of BPDs, including Burgers vectors, running directions, glide type, and the classification by Iijima et al.[36] In reference to Table I, DRSF-A and DRSF-B are classified as #2 and #6, respectively. In all cases in Table I, the ***b*** of the original BPDs is

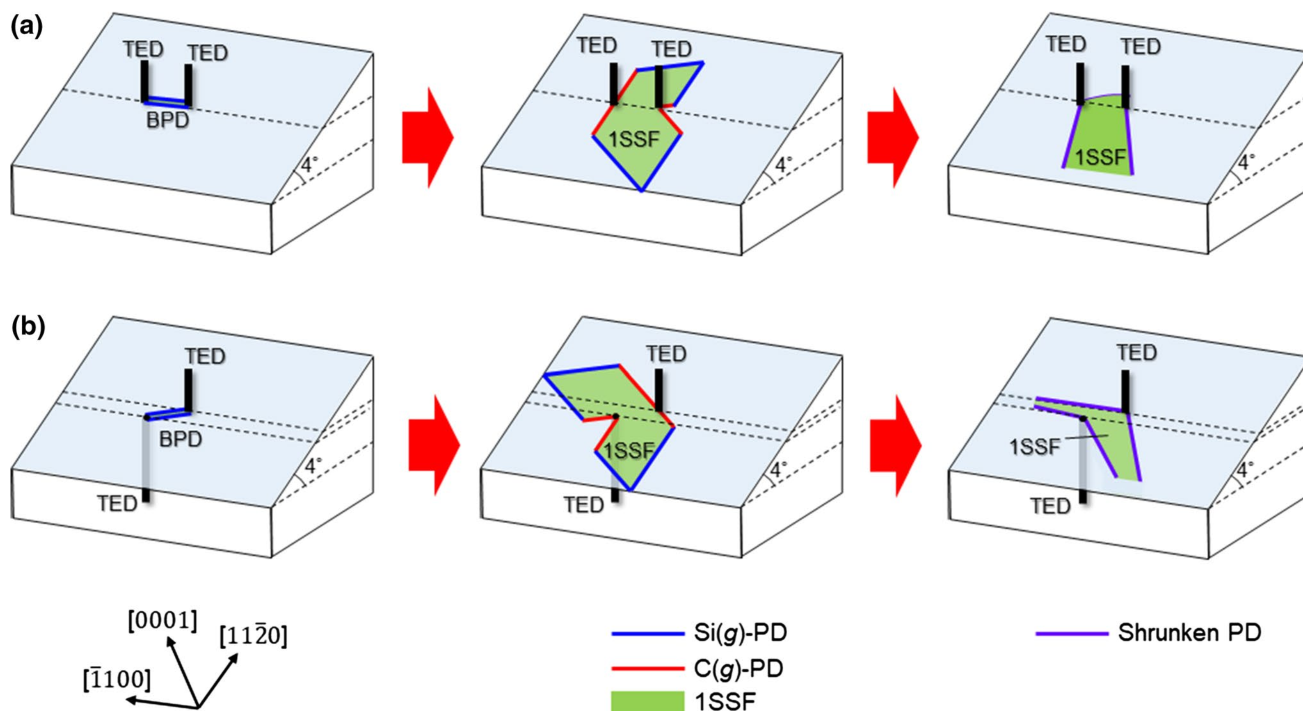

Fig. 9 Three-dimensional schematics of DRSFs from unexpanded BPD, expanded by UV illumination, and shrunken during FIB sample preparation or TEM observation: (a) DRSF-A, and (b) DRSF-B.

found to be 60 degrees to the running directions. Only when giant $\pm(\bar{1}100)$ steps were formed, trans-configuration TEDs would be possible even for #1 and #2 DRSFs. In reality, there seems to be no chance for the $\pm(\bar{1}100)$ steps to be bunched to form very high steps during chemical vapor deposition epitaxial growth, because off-cut oriented steps flow toward $[11\bar{2}0]$. Therefore, trans-configuration TEDs are extremely unlikely for #1 or #2 DRSFs.

Conclusions

We investigated the structure of the DRSFs to identify Burgers vectors, core species, and the type of glide of the constituent PDs by plan-view TEM and cross-sectional HAADF-STEM. From the results, we found that there are two types of DRSFs; one is an HLA-oriented type for which the Burgers vector of the original BPD is $\pm(1/3)[11\bar{2}0]$ and cis-configuration of TEDs on both ends and the other is isolated and inclined for which the Burgers vector of the original BPD is $\pm(1/3)[\bar{2}110]$ or $\pm(1/3)[1\bar{2}10]$ and trans-configuration of TEDs on both ends. The procedure for determining the type of glide is described by directly observing the facing of the tetrahedrons experimentally on the faulted basal planes using high-resolution HAADF-STEM images acquired on any $(11\bar{2}0)$ planes. In both cases of DRSFs, the feature of the original BPDs was found to be perfect 60-degree dislocations even consisting of possible combinations of two running directions.

The shrinking process of the DRSFs was also examined and it was found that it was not a reversal of the expansion process. This implies that the expansion criteria are no longer useful for distinguishing mobile Si-core and immobile C-core PDs in the shrinking process. When observing the shrinking 1SSF shape, we need to be very careful to judge the core species just by the way they contract.

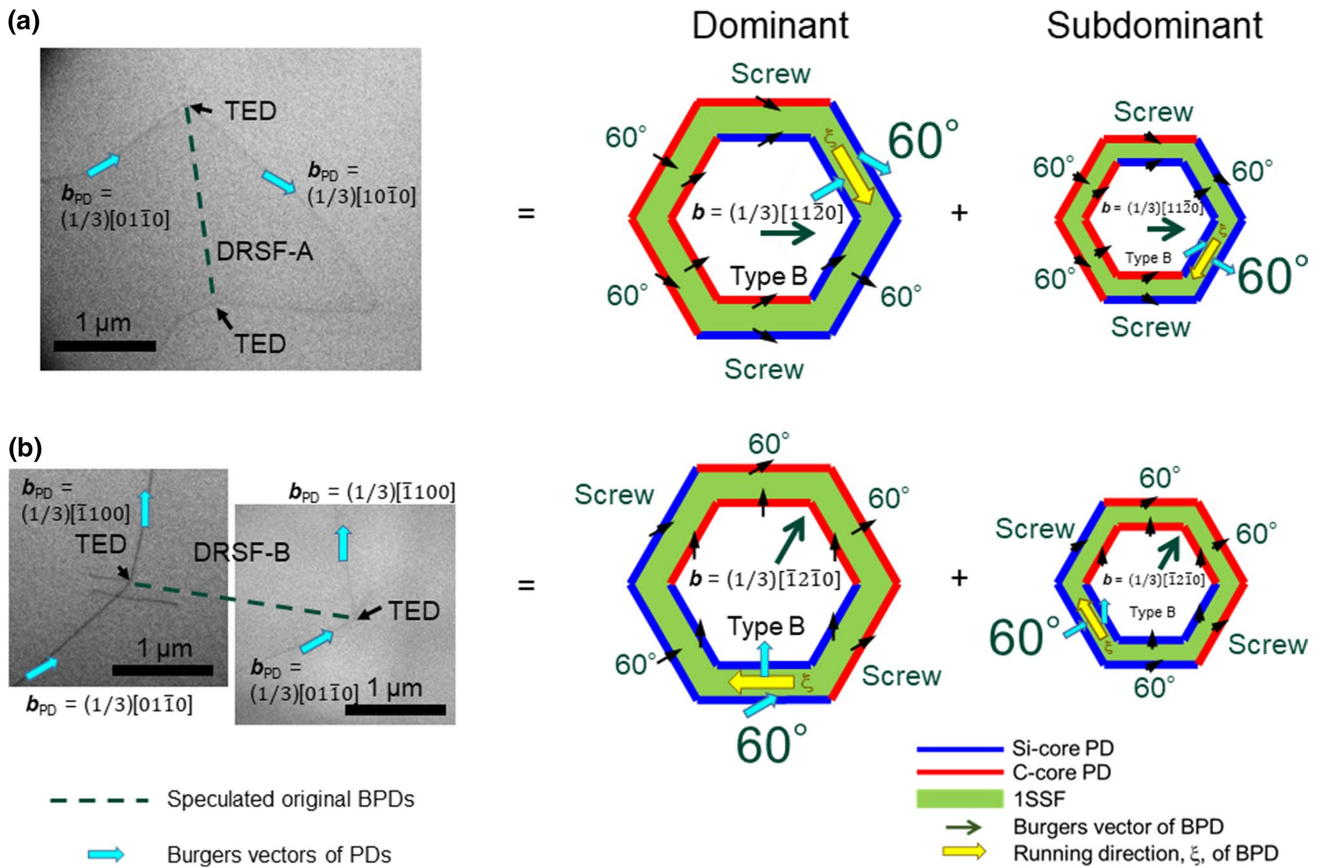

Fig. 10 Plan-view BF-TEM images of DRSFs and results of Burgers vectors of PDs and estimated original BPDs with comprehension by unexpanded BPD dislocation loops: (a) DRSF-A and (b) DRSF-B.

Table 1 Schematic DRSF shapes, corresponding structures of original BPDs, and configuration of TEDs on both ends of the BPD

Schematic DRSF shapes ($[\bar{1}100]$, $[11\bar{2}0]$, $[0001]$)	BPD structure			
	Burgers vector	Running direction, ξ	Type	Classification by Iijima, et al.
#1	±(1/3)[11$\bar{2}$0]	±[1$\bar{2}$10] ±[2$\bar{1}\bar{1}$0]	A	(a5) (a6)
#2	±(1/3)[11$\bar{2}$0]	±[1$\bar{2}$10] ±[2$\bar{1}\bar{1}$0]	B	(a11) (a12)
#3	±(1/3)[$\bar{2}$110]	±[11$\bar{2}$0] ±[$\bar{1}$2$\bar{1}$0]	A	(a13) (a14)
#4	±(1/3)[$\bar{2}$110]	±[11$\bar{2}$0] ±[$\bar{1}$2$\bar{1}$0]	B	(a19) (a20)
#5	±(1/3)[1$\bar{2}$10]	±[$\bar{2}$110] ±[$\bar{1}\bar{1}$20]	A	(a27) (a28)
#6	±(1/3)[1$\bar{2}$10]	±[$\bar{2}$110] ±[$\bar{1}\bar{1}$20]	B	(a33) (a34)

Conflict of interest The authors declare that they have no conflict of interest.

References

1. T. Ishigaki, T. Murata, K. Kinoshita, T. Morikawa, T. Oda, R. Fujita, K. Konishi, Y. Mori, and A. Shima, Analysis of Degradation Phenomena in Bipolar Degradation Screening Process for SiC-MOSFETs. In: Proceeding 31st international symposium power semiconductor devices and ICs, p. 259 (2019).
2. T. Tawara, T. Miyazawa, M. Ryo, M. Miyazato, T. Fujimoto, K. Takenaka, S. Matsunaga, M. Miyajima, A. Otsuki, Y. Yonezawa, T. Kato, H. Okumura, T. Kimoto, and H. Tsuchida, Short minority carrier lifetimes in highly nitrogen-doped 4H-SiC epilayers for suppression of the stacking fault formation in PiN diodes. *J. Appl. Phys.* 120, 115101 (2016).
3. A. Tanaka, H. Matsuhata, N. Kawabata, D. Mori, K. Inoue, M. Ryo, T. Fujimoto, T. Tawara, M. Miyazato, M. Miyajima, K. Fukuda, A. Ohtsuki, T. Kato, H. Tsuchida, Y. Yonezawa, and T. Kimoto, Growth of Shockley type stacking faults upon forward degradation in 4H-SiC P-i-N diodes. *J. Appl. Phys.* 119, 095711 (2016).
4. S. Hayashi, T. Yamashita, J. Senzaki, M. Miyazato, M. Ryo, M. Miyajima, T. Kato, Y. Yonezawa, K. Kojima, and H. Okumura, Influence of basal-plane dislocation structures on expansion of single Shockley-type stacking faults in forward-current degradation of 4H-SiC P-i-N diodes. *Jpn. J. Appl. Phys.* 57, 04FR07 (2018).
5. J. Nishio, A. Okada, C. Ota, and R. Iijima, Direct confirmation of structural differences in single Shockley stacking faults expanding from different origins in 4H-SiC PiN diodes. *J. Appl. Phys.* 128, 085705 (2020).
6. J. Nishio, A. Okada, C. Ota, and R. Iijima, Single Shockley stacking fault expansion from immobile basal plane dislocations in 4H-SiC. *Jpn. J. Appl. Phys.* 60, SBBD01 (2021).
7. J. Nishio, C. Ota, and R. Iijima, Conversion of Shockley partial dislocation pairs from unexpandable to expandable combinations after epitaxial growth of 4H-SiC. *J. Appl. Phys.* 130, 075107 (2021).
8. C. Ota, J. Nishio, A. Okada, and R. Iijima, Origin and generation process of a triangular single Shockley stacking fault expanding from the surface side in 4H-SiC PIN diodes. *J. Electron. Mater.* 50, 6504 (2021).
9. J. Nishio, C. Ota, and R. Iijima, Structural study of single Shockley stacking faults terminated near substrate/epilayer interface in 4H-SiC. *Jpn. J. Appl. Phys.* 61, SC1005 (2022).
10. S. Ha, H.J. Chung, N.T. Nuhfer, and M. Skowronski, Dislocation nucleation in 4H silicon carbide epitaxy. *J. Cryst. Growth* 262, 130 (2004).
11. S. Ha, M. Skowronski, and H. Lendenmann, Nucleation sites of recombination-enhanced stacking fault formation in silicon carbide P-i-N diodes. *J. Appl. Phys.* 96, 393 (2004).
12. X. Zhang, S. Ha, Y. Hanlumnyang, C.H. Chou, V. Rodriguez, M. Skowronski, J.J. Sumakeris, M.J. Paisley, and M.J. O'Loughlin, Morphology of basal plane dislocations in 4H-SiC homoepitaxial layers grown by chemical vapor deposition. *J. Appl. Phys.* 101, 053517 (2007).
13. Z. Zhang, R.E. Stahlbush, P. Pirouz, and T.S. Sudarshan, Characteristics of dislocation half-loop arrays in 4H-SiC homo-epilayer. *J. Electron. Mater.* 36, 539 (2007).
14. X. Zhang, M. Skowronski, K.X. Liu, R.E. Stahlbush, J.J. Sumakeris, M.J. Paisley, and M.J. O'Loughlin, Glide and multiplication of basal plane dislocations during 4H-SiC homoepitaxy. *J. Appl. Phys.* 102, 093520 (2007).
15. H. Tsuchida, I. Kamata, K. Kojima, K. Momose, M. Odawara, T. Takahashi, Y. Ishida, and K. Matsuzawa, Influence of growth conditions and substrate properties on formation of interfacial dislocations and dislocation half-loop arrays in 4H-SiC (0001) and (000–1) epitaxy. *MRS Symp. Proc.* (2008). https://doi.org/10.1557/PROC-1069-D04-03.
16. N. Zhang, Y. Chen, Y. Zhang, M. Dudley, and R.E. Stahlbush, Nucleation mechanism of dislocation half-loop arrays in 4H-silicon carbide homoepitaxial layers. *Appl. Phys. Lett.* 94, 122108 (2009).
17. R.E. Stahlbush, B.L. VanMil, K.X. Liu, K.K. Lew, R.L. Myers-Ward, D.K. Gaskill, C.R. Eddy Jr., X. Zhang, and M. Skowronski, Evolution of basal plane dislocations during 4H-SiC epitaxial growth. *Mater. Sci. Forum* 600–603, 317 (2009).
18. S. Ha, M. Benamara, M. Skowronski, and H. Lendenmann, Core structure and properties of partial dislocations in silicon carbide P-i-N diodes. *Appl. Phys. Lett.* 83, 4957 (2003).
19. R.E. Stahlbush, M.E. Twigg, J.J. Sumakeris, K.G. Irvine, and P.A. Losee, Mechanisms of stacking fault growth in SiC PiN diodes. *MRS Symp. Proc.* 815, J6.4 (2004).
20. B. Chen, T. Sekiguchi, T. Ohyanagi, H. Matsuhata, A. Kinoshita, and H. Okumura, Electron-beam-induced current and cathodeluminescence study of dislocation arrays in 4H-SiC homoepitaxial layers. *J. Appl. Phys.* 106, 074502 (2009).
21. J. Nishio, C. Ota, and R. Iijima, Transmission electron microscopy study of single Shockley stacking faults in 4H-SiC expanded from basal plane dislocation segments accompanied by threading edge dislocations on both ends. *Mater. Sci. Forum* 1062, 258 (2022).
22. J. Nishio, A. Okada, C. Ota, and M. Kushibe, Photoluminescence analysis of individual partial dislocations in 4H-SiC epilayers. *Mater. Sci. Forum* 1004, 376 (2020).
23. J. Nishio, A. Okada, C. Ota, and M. Kushibe, Triangular single Shockley stacking fault analyses on 4H-SiC PiN diode with forward voltage degradation. *J. Electron. Mater.* 49, 5232 (2020).
24. S.G. Sridhara, F.H.C. Carlsson, J.P. Bergman, and E. Janzén, Luminescence from stacking faults in 4H SiC. *Appl. Phys. Lett.* 79, 3944 (2001).
25. R.E. Stahlbush, Q. Zhang, A. Agarwal, and N.A. Mahadik, Effect of stacking faults originating from half loop arrays on electrical behavior of 10 kV 4H-SiC PiN diodes. *Mater. Sci. Forum* 717–720, 387 (2012).
26. N.A. Mahadik, R.E. Stahlbush, J.D. Caldwell, and K.D. Hobart, Ultraviolet photoluminescence imaging of stacking fault contraction in 4H-SiC epitaxial layers. *Mater. Sci. Forum* 717–720, 391 (2012).
27. H. Matsuhata, H. Yamaguchi, T. Yamashita, T. Tanaka, B. Chem, and T. Sekiguchi, Contrast analysis of Shockley partial dislocations in 4H-SiC observed by synchrotron Berg-Barrett X-ray topography. *Philos. Mag.* 94, 1674 (2014).
28. H. Matsuhata and T. Sekiguchi, Morphology of single Shockley-type stacking faults generated by recombination enhanced dislocation glide in 4H-SiC. *Philos. Mag.* 98, 878 (2018).
29. T. Tanaka, H. Shiomi, N. Kawabata, Y. Yonezawa, T. Kato, and H. Okumura, Expansion and contraction of single Shockley stacking faults in SiC epitaxial layer under ultraviolet irradiation. *Appl. Phys. Express* 12, 041006 (2019).
30. A. Okada, J. Nishio, R. Iijima, C. Ota, A. Goryu, M. Miyazato, M. Ryo, T. Shinohe, M. Miyajima, T. Kato, Y. Yonezawa, and H. Okumura, Dependences of contraction/expansion of stacking faults on temperature and current density in 4H-SiC P-i-N diodes. *Jpn. J. Appl. Phys.* 57, 061301 (2018).
31. M.E. Twigg, R.E. Stahlbush, M. Fatemi, S.D. Arthur, J.B. Fedison, J.B. Tucker, and S. Wang, Structure of stacking faults formed during the forward bias of 4H-SiC P-i-N diodes. *Appl. Phys. Lett.* 82, 2410 (2003).

32. M. Zhang, P. Pirouz, and H. Lendenmann, Transmission electron microscopy investigation of dislocations in farward-biased 4H-SiC P-i-N diodes. *Appl. Phys. Lett.* 83, 3320 (2003).
33. Y. Ishikawa, M. Sudo, Y.-Z. Yao, Y. Sugawara, and M. Kato, Expansion of a single Shockley stacking fault in a 4H-SiC (11 0) epitaxial layer caused by electron beam irradiation. *J. Appl. Phys.* 123, 225101 (2018).
34. P. Pirouz, J.L. Demenet, and M.H. Hong, On transition temperatures in the plasticity and fracture of semiconductors. *Philos. Mag. A* 81, 1207 (2001).
35. M. Skowronski, J.Q. Lui, W.M. Vetter, M. Dudley, C. Hallin, and H. Lendenmann, Recombination-enhanced defect motion in forward-biased 4H-SiC *p-n* diodes. *J. Appl. Phys.* 92, 4699 (2002).
36. A. Iijima, I. Kamata, H. Tsuchida, J. Suda, and T. Kimoto, Correlation between shapes of Shockley stacking faults and structures of basal plane dislocations in 4H-SiC epilayers. *Philos. Mag.* 97, 2736 (2017).

Publisher's Note Springer Nature remains neutral with regard to jurisdictional claims in published maps and institutional affiliations.